PII: S1359-8368(96)00077-7

Fracture strength and damage progression of the fiber/matrix interfaces in titanium-based MMCs with different interfacial layers

Leon L. Shaw[a,*], Prasanna Karpur[b] and Theodore E. Matikas[b]

[a]Department of Metallurgy, Institute of Materials Science, University of Connecticut, Storrs, CT, USA
[b]Research Institute, University of Dayton, Dayton, OH, USA

In this paper, a concerted utilization of finite element analysis and an ultrasonic characterization technique is described to assess the interfacial fracture strength and to monitor the progression of damage at the interfacial region in titanium-based metal-matrix composites. The finite element model developed here encompasses an interfacial element with a finite thickness to simulate the interfacial region of the coating or reaction products. The finite element model has been used in conjunction with the ultrasonic evaluation technique to assess the *in situ* interfacial fracture strength. The different responses of the ultrasonic amplitudes for Ti–6Al–4V/SCS-0 SiC and Ti–6Al–4V/SCS-6 SiC interfaces have been explained in terms of the reflection of ultrasonic waves from the fiber/matrix interface. It is established that the non-monotonic stress dependence of the ultrasonic reflection amplitude for both the SCS-0 and SCS-6 interfaces is related to the debonding between the fiber and matrix. The results indicate that the SCS-0 interface has a much higher fracture strength than the SCS-6 interface although both these interfaces exhibit similar apparent debonding stresses. © 1998 Elsevier Science Limited. All rights reserved

INTRODUCTION

The macroscopic behavior of metal-matrix composites (MMCs) is related to the properties of the fiber/matrix interface. It is at the interface that the load transfer takes place and the crack deflection exists. As a result, characterization of the interfacial properties and their influence on the properties of MMCs are of great interest to researchers developing MMCs. Various techniques have been developed to characterize the interfacial properties in MMCs. Examples of these characterization techniques are composite cylinder specimens[1], fiber pull-out tests[1-3], fiber push-out tests[2,4], tensioned push-out tests[5], slice compression tests[6] and fiber fragmentation[7-10]. Most of these tests are designed to measure the shear strength of the fiber/matrix interface. In contrast, relatively few tests are designed for *in situ* measurement of the tensile (normal) fracture strength of the fiber/matrix interface. Typically, the normal strength of the interface can be measured through transverse loading conditions. However, one major problem associated with the measurement of interfacial strength under transverse loading is the presence of the singularity at the free surface (where the fiber tip intersects the surface of the composite). This singularity is induced during cooling of MMCs from the processing temperatures[11-13], and causes

interfacial debonding either at a much lower stress level than the value required for the same failure to commence at the interior of the composite[11] or even when no external stresses are applied[12,14,15]. As a result, observations made on the free surface of the composites may not be representative of the behavior in the interior of MMCs. Furthermore, most of the aforementioned characterization techniques are unsuitable for *in situ* monitoring of the failure of the interface and the progression of interfacial damage during service. Therefore, a technique capable of measuring the interfacial strength as well as monitoring the failure of the interface and the progression of interfacial damage *in situ* is very desirable. Hence, a new technique was developed to monitor the behavior of the interfaces in the interior of the composites under transverse loading conditions[15,16].

This paper reports a new method[15,16] to assess the interfacial fracture strength and monitor the progression of damage at the interfacial region in titanium-based MMCs. The method is based on a recently developed ultrasonic technique, called the shear wave back-reflectivity technique (SBR)[17-19]. This technique, which uses an ultrasonic shear wave, has been demonstrated to be much more sensitive to the interfacial conditions than ultrasonic imaging techniques using longitudinal waves[19], and was successfully used to evaluate the fiber/matrix interfacial 'shear stiffness coefficient', matrix texture, consolidation quality,
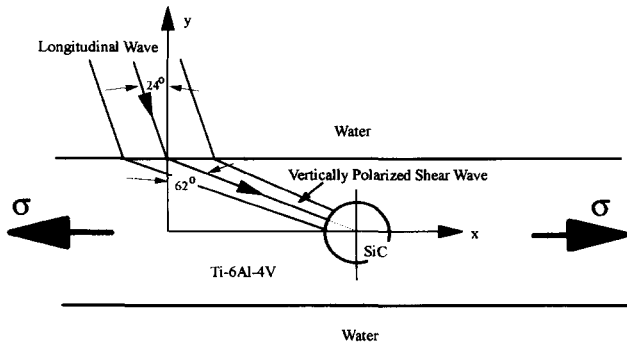

Figure 1 Test set-up for ultrasonic imaging. The 62° orientation of the shear wave with respect to the normal of the water/Ti-6-4 interface is based on the law of refraction

high-temperature degradation of MMCs and fiber fracture in matrices[9,17–21]. More recently, the images of the SBR have been shown to be related to the debonding and interfacial separation between the fiber and matrix in titanium-based MMCs under transverse loading[14]. Therefore, the SBR has provided useful information about the onset of interfacial debonding and interfacial separation in the interior of the composites as a function of the transverse loading. In this paper, the SBR technique is applied to Ti–6Al–4V/SiC composites with different interfacial conditions. The sensitivity of the ultrasonic images to the interfacial conditions are investigated and, in conjunction with finite element modeling, the *in situ* interfacial strength under transverse loading is assessed.

The ultrasonic shear wave back-reflectivity technique is based on interrogation of the interface in a pulse-echo mode with an ultrasonic shear wave[17–19]. The shear wave used in the SBR is produced by the incidence of a longitudinal ultrasonic wave on titanium-based MMCs at a suitable angle (for titanium-based alloys this angle is 24°, which is between the first and the second critical angles* for titanium materials), as shown in *Figure 1*. Since the wave front is incident at an angle, the received back-reflected signal is either low amplitude owing to back-scattering from the matrix grain structure or high amplitude owing to back-reflection from the fiber/matrix interface (when the wave front is perpendicular to the fiber circumference). This amplitude variation along the length of the fiber characterizes the fiber/matrix interface because the amplitude of the back-reflected wave is determined by the reflection coefficient, R, of the wave at the interface and also by the slope of the debond surface†([14]).

EXPERIMENTAL PROCEDURES

The samples used in this study were Ti–6Al–4V composites

---

* The first critical angle is the incident angle at which compressional ultrasonic waves cease to propagate in titanium. The second critical angle is the incident angle at which shear or tangential waves also cease to propagate in titanium

† The slope of the debond surface is the angle of an imaginary line drawn as a tangent to the curvature produced by the matrix which has debonded from the fiber and has undergone some distortion due to the loading process

containing a single SiC fiber. The purpose of using single-fiber composites was to avoid the fiber interactions in high-volume-fiber composites. Therefore, the intrinsic phenomena related to the interfacial fracture and deformation could be studied with clarity. The composites were fabricated by hot pressing two Ti–6Al–4V sheets with a single SiC fiber at 930°C with 17 MPa for 2 h. After the consolidation, several different cooling conditions were used to alter the residual thermal stresses (see *Table 1*). To prevent damage to the fiber surface during consolidation, the single fiber was aligned before hot pressing by placing it in a fiber retention groove in one of the titanium sheets. The groove depth was the same as the fiber diameter (142 μm) and was introduced through a specially constructed shaping apparatus. The fiber used was either SCS-6 or SCS-0 series. In the case of SCS-6 fibers, there was a graded carbon/silicon coating on the surface of the fiber. This coating will be called as the carbon coating in the following text for brevity of writing. For SCS-0 fibers, no coating existed on the fiber surface and reaction products were formed in between the fiber and matrix during the hot consolidation of the composites. Some composites containing two widely separated SCS-0 and SCS-6 fibers were fabricated, thereby facilitating comparison of the ultrasonic responses of these two fibers to the transverse loading. The difference between the SCS-6 and SCS-0 interfaces is that the former has a carbon coating, while the latter has reaction products at the interface consisting of titanium silicides and carbides[22].

The consolidated samples were cut into a dogbone shape with the fiber axis perpendicular to the loading axis of the samples. Transverse tensile tests were carried out on a micro-straining stage built in our laboratory[10] to facilitate loading under water so that ultrasonic evaluation could be conducted *in situ* during the loading process. The loading was applied stepwise so that the ultrasonic scanning could be carried out under the loaded condition at different stress levels. The experimental set-up for ultrasonic imaging has been shown in *Figure 1*. The transversely loaded composite specimen was immersed in water and imaged mode converted a vertically polarized shear wave which was incident on the fiber/matrix interface. A 25 MHz focused ultrasonic transducer was used in this work.

FINITE ELEMENT MODELING

It has been shown that the presence of an interfacial region (coating or reaction products) has a strong effect on the interfacial crack initiation and propagation[23]. Therefore, the present finite element analysis (FEA) encompassed an interfacial region with a finite thickness and independent thermal and mechanical properties. The FEA was implemented by using the ANSYS code[24]. The fiber and matrix were described with three-dimensional, eight-noded isoparametric elements, while the interfacial region was simulated with three-dimensional, eight-noded concrete solids. The isoparametric elements have the capability of plasticity if needed, and the concrete solids are similar to the isoparametric elements but with the addition of cracking

Table 1 Interfacial fracture strength estimated from finite element analysis for Ti–6Al–4V/SiC composites with different interfacial conditions

Interfacial conditions	Post-consolidation cooling conditions[a]	Stress level at which the decrease in ultrasonic amplitude starts (MPa)	Assumed interfacial tensile fracture strength *versus* compressive strength in FEA (MPa)	Crack initiation stress predicted from FEA (MPa)
SCS-6	500°C/WQ to RT	~300	100 *versus* 1000	180
			200 *versus* 1000	240
			300 *versus* 1000	300
SCS-6	930°C/FC to RT	~300	100 *versus* 1000	180
			200 *versus* 1000	240
			300 *versus* 1000	300
SCS-0	930°C/FC to RT	~300	600 *versus* 3000	100
			700 *versus* 3000	190
			800 *versus* 3000	280
SCS-0	500°C/FC to RT	~400	800 *versus* 3000 MPa with the assumed 300°C WQ	430
			800 *versus* 3000 MPa with the assumed 400°C WQ	350

[a]WQ = Water quenched; FC = furnace cooled; RT = room temperature

and crushing capabilities. The cracking and crushing capabilities of the concrete solids are necessary to assess the interfacial crack initiation and propagation. The criterion for failure of the concrete solids (cracking and/or crushing) under multiaxial stresses is expressed in ANSYS as[24]

$$\frac{F}{f_c} - S \geq 0 \tag{1}$$

where F is a function of the principal stresses $(\sigma_1, \sigma_2, \sigma_3), f_c$ is the uniaxial crushing strength, and S is the failure surface expressed in terms of the principal stresses and material properties of the concrete solid. If eqn (1) is satisfied, the concrete solid will crack or crush, depending on the stress state. The solid cracks if any principal stress is tensile, while crushing occurs only if all principal stresses are compressive. Details of the function, F, and the failure surface, S, can be found in the ANSYS manual[24]. However, when all principal stresses are tensile, eqn (1) is reduced to

$$\frac{\sigma_i}{f_c} - \frac{f_t}{f_c} \geq 0, \quad i = 1, 2, 3 \tag{2}$$

where f_t is the uniaxial tensile fracture strength. In this case the occurrence of cracking is simply based on the magnitudes of the maximum tensile stresses. This is a reasonable criterion for the interfacial region present in this study because, as will be discussed below, the interfacial regions in this study are composed of brittle materials. When both the tensile and compressive stresses are present, cracking stresses will be reduced accordingly as shown in *Figure 2*, where the failure surface is presented for $\sigma_3 = 0$. For the present study, there was always one tensile stress component and the uniaxial crushing strength (f_c) was set to be very high. As a result, only cracking occurred and it always happened at a stress level equal or close to the uniaxial tensile fracture strength. In the ANSYS code, cracking is allowed to occur in the planes perpendicular to three principal stresses independently and treated by introducing a plane of weakness in a direction normal to the cracked plane. Thus, a cracked body can still sustain tensile stresses in the other two orthogonal directions and transmits shear and compressive stresses in the cracked plane if the crack is

forced to close. After a crack initiates, no singularity at the crack tip has been treated in this study. Instead, the crack-tip stresses are averaged over the entire element adjacent to the crack, leading to a size dependence of the stresses in the element adjacent to the crack. Therefore, the prediction for the crack initiation stress is rigorous in this study, while the prediction for the crack propagation stress should be considered with caution.

The finite element mesh used is shown in *Figure 3*. The fiber diameter was set to be 140 μm, the typical diameter of SCS-6 and SCS-0 SiC fibers. The composite was assumed to be infinite in the direction of fiber axis (i.e. the z-coordinate direction). In the y-direction the composite was assumed to have a thickness of 2 mm corresponding to the actual thickness of the test specimens. In the direction perpendicular to the fiber axis (i.e. the x-direction), a length of 4 mm was assumed. This is believed to be sufficient for the simulation of the test specimens, because at the distance of about three times the fiber diameter from the fiber, the stresses in the matrix are almost uniform[25]. The interface
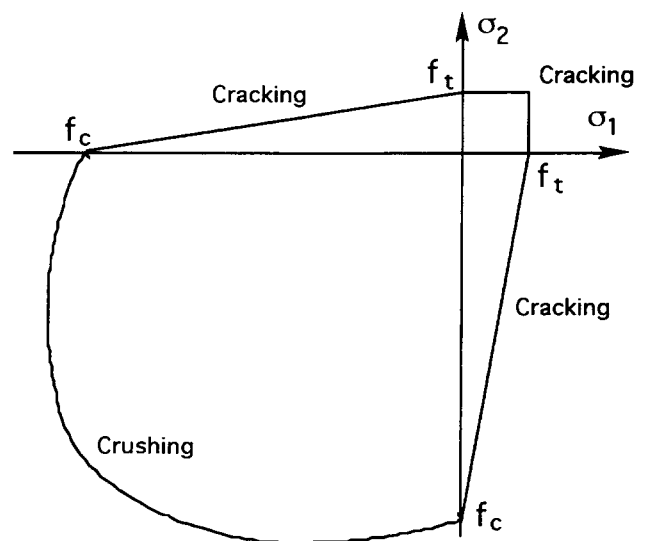

Figure 2 Schematic of the failure surface of the concrete solids at $\sigma_3 = 0$. f_t and f_c are the uniaxial tensile fracture and crushing strengths, respectively
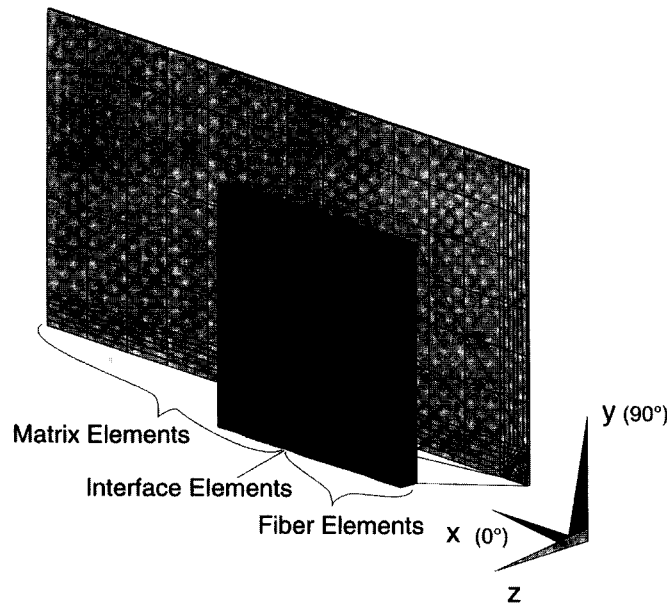
Figure 3 Finite element mesh used to model single-fiber composites. The transverse load is applied along the *x*-axis

was assumed to have a thickness of 1 μm to represent the coating or reaction products. The 1 μm thickness was chosen arbitrarily, because it has been demonstrated[23] that the interfacial crack initiation and propagation are not affected by the thickness of the coating when the coating is within a typical thickness range (0.5 to 3.0 μm). The boundary conditions in this study were set in such a way that one-eighth of the composite could be used to represent the behavior of the whole composite. Specifically, the nodes on the bottom face of the model (i.e. the *x*–*z* plane at $y = 0$) were not allowed to move in the *y*-direction, while the nodes on the top face of the model were free to move. The nodes on the *y*–*z* plane at $x = 0$ were not allowed to move in the *x*-direction, while the nodes on the *y*–*z* plane at $x = 2$ were coupled together to move the same distance in the *x*-direction. Similarly, the nodes on the back face of the model (i.e. the *x*–*y* plane at $z = 0$) were not allowed to move in the *z*-direction, while the nodes on the front face of the mode were coupled in the *z*-direction.

The input properties of various constituents are summarized in *Table 2*. The SiC fiber was assumed to be elastic with isotropic and homogeneous properties, while the matrix was treated as an isotropic and homogeneous material with plasticity. Because of the difficulty of measuring the *in situ* properties of the interracial region, it was assumed that the properties of this region were dominated by the major phase

in the interfacial region and its properties were similar to those of its corresponding bulk material. Thus, for the carbon-coated interfacial region, the elastic modulus and the coefficient of thermal expansion were assumed to be the mean values of C/C composites[26,27]. For the uncoated interfacial region, since it has been established that titanium carbides and silicides are formed between the fiber and matrix during consolidation[22], the interfacial region was assumed to have the elastic and thermal properties of TiC bulk material.

Both thermal and transverse mechanical loads were considered in this study. The zero stress state of the composites was assumed to be at the post-consolidation annealing temperatures. Thermal loads were applied under the assumption that the temperature is spatially uniform throughout the composites. The composites were assumed to be quenched from the annealing temperature to 25°C. Therefore, no time-dependent stress relaxation during cooling was considered. Obviously, if time-dependent relaxation were considered, lower residual stresses would result. The difference between the time-dependent and time-independent conditions has been evaluated by Nimmer *et al.*[28], who have estimated a 16% reduction of the room-temperature residual effective stress in Ti–6Al–4V/SiC composites as a result of time-dependent relaxation behavior for a cooling rate of 2300°C h^{-1} from 900 to

Table 2 Parameters of Ti–6Al–4V/SiC composites related to ultrasonic testing and finite element modeling

Material	Elastic modulus (GPa)	Coefficient ofthermal expansion (10^{-6} °C^{-1})	Density (g cm^{-3})	Yield strength (MPa)	Shear wave velocity (cm s^{-1})	Acoustic impedance (N s m^{-3})
Ti–6Al–4V[24]	113.8	9.8	4.43	890[a]	3.12 × 10^5	1.381 × 10^7
SiC[25]	414.0	4.86	3.2	—	6.96 × 10^5	2.227 × 10^7
Carbon[26,27]	100.0	4.86	2.25	—	4.08 × 10^5	9.185 × 10^6
TiC[28,29]	310	7.4	4.94	—	4.85 × 10^5	2.396 × 10^7
Water[30]	—	—	1.0	—	1.44 × 10^5 [b]	1.44 × 10^6

[a]The post-yield stress–strain relationship: $\sigma = 881 + 2085\epsilon$ (MPa)[21]
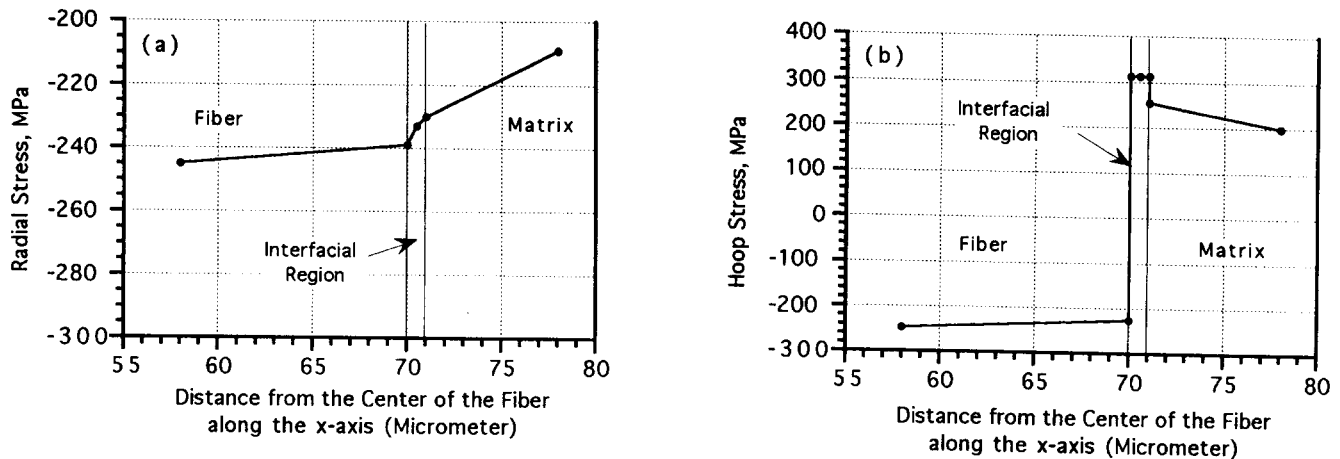[b]Longitudinal wave velocity

Figure 4 Residual thermal stresses near the interfacial region for a SCS-0 composite after cooling from 500 to 20°C: (a) radial stresses; (b) hoop stresses

25°C. Thus, if the same difference was assumed, then for a quenching from 500°C to 25°C, the present study might overestimate residual stresses by about 6–8% with a gain of computational time. For the specimens furnace-cooled from 930°C (see *Table 1*), it was assumed that 930°C furnace cooling was equivalent to 500°C water quenching, because the SCS-6 composites with these two cooling conditions exhibited similar stress levels for the onset of the decrease in the ultrasonic amplitude (to be discussed in detail in Section Section 4). For the composites furnace-cooled from 500°C, the residual thermal stresses were certainly lower than those in the composites water-quenched from 500°C. However, since the equivalent quenching temperature was not clear, two different quenching temperatures (see *Table 1*) were evaluated to examine the effect of the residual thermal stresses.

After the cooling event, the mechanical load was super-imposed onto the residual thermal stresses by applying a transverse stress in the *x*-coordinate direction. During the loading, if eqn (1) was satisfied at any location of the interfacial region, an interfacial crack would initiate at that specific location and it might propagate instantly or gradually along the interfacial region depending on the stresses in the adjacent interfacial region (to be discussed further in the Results and Discussion section). After cracking, the interfacial region could still transmit compressive and shear stresses. The transmission of shear stresses was achieved by assigning a shear transfer coefficient at the closed cracked plane. A coefficient of '1' corresponds to a perfect transfer while '0' corresponds to no transfer. In this study, a coefficient of 0.5 was assumed arbitrarily because it has been shown that the choice of a Coulomb friction coefficient for a cracked interface does not play a strong role in the predicted transverse stress–strain behavior of Ti–6Al–4V/SiC composites[29].

RESULTS AND DISCUSSION

Finite element analysis

As expected, the FEA reveals that for both the interfacial

conditions studied, as the tensile fracture strength of the interfacial region increases, the stress for the initiation of an interfacial crack increases (*Table 1*). However, there are some detailed differences between these two composites. These include differences in the intrinsic fracture strength of the interface, the residual thermal stresses at the interfacial region, and the initiation and propagation of the interfacial crack.

Residual thermal hoop and radial stresses near the interfacial region for the SCS-0 and SCS-6 composites at the as-quenched condition (from 500°C to 25°C) are shown in *Figures 4* and *5*, respectively. As expected, the larger coefficient of thermal expansion (CTE) of the matrix compared with the fiber creates a tensile hoop stress and a compressive radial stress in the matrix near the fiber/matrix interface. Furthermore, the magnitudes of these stresses are almost independent of the composite systems, suggesting that the effect of the interfacial properties on the residual thermal stresses within the matrix and the fiber is small. This is believed to be due to the small thickness of the interfacial region compared with the matrix and fiber. However, the residual stresses within the interfacial region are quite different for the two composites. For the SCS-0 composite, the interfacial region has a residual tensile hoop stress because of its higher CTE than that of the fiber. In contrast, the residual hoop stress in the interfacial region of the SCS-6 composite is compressive because its CTE is lower than that of the matrix. The residual radial stresses are almost the same for both composites, indicating that the radial stresses are dominated by the CTE mismatch between the matrix and fiber. Finally, it is noted that the hoop and radial stresses near the interface are very similar along the *x*- and *y*-axis directions (not shown in the figures), suggesting a small effect of the matrix dimension on the residual stresses at the interface. This is due to the much larger dimensions of the matrix compared with the dimensions of the fiber.

The compressive radial stresses at the interface for the both composites provide a clamping stress against inter-facial debonding at 0° with respect to the transverse tensile axis (i.e. the *x*-direction, *Figure 3*) during the loading.

(a)

Radial Stress, MPa

-200
-220
-240
-260
-280
-300

Fiber　　Matrix

Interfacial Region

55　60　65　70　75　80

Distance from the Center of the Fiber along the x-axis (Micrometer)

(b)

Hoop Stress, MPa

400
300
200
100
0
-100
-200
-300

Interfacial Region

Fiber　　Matrix

55　60　65　70　75　80

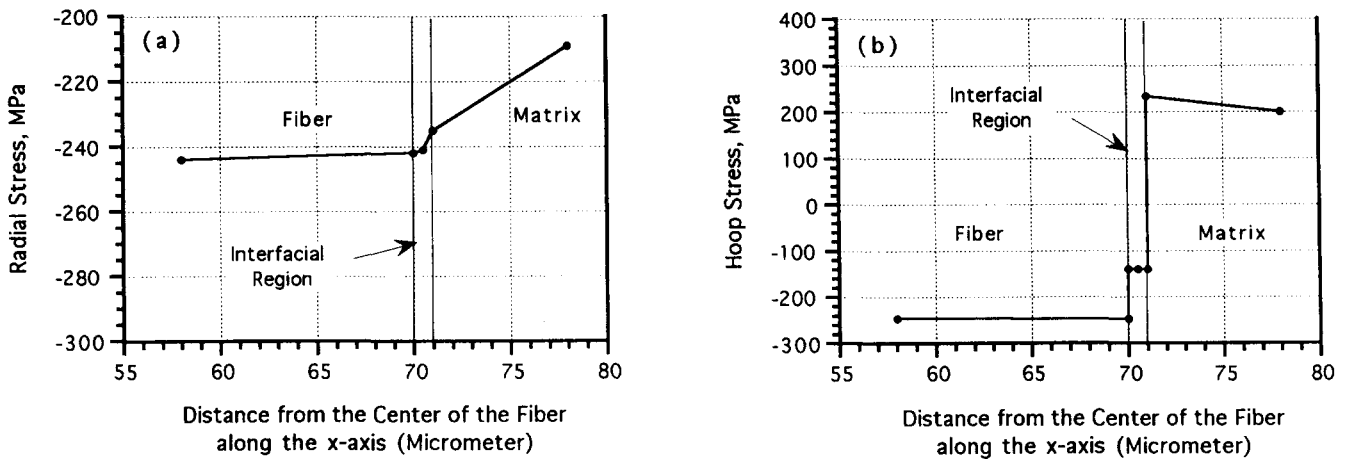Distance from the Center of the Fiber along the x-axis (Micrometer)

Figure 5　Residual thermal stresses near the interfacial region for a SCS-6 composite after cooling from 500 to 20°C: (a) radial stresses; (b) hoop stresses

However, the tensile hoop stress in the interfacial region for the SCS-0 composite tends to enhance radial cracking at 90° during the transverse loading. Because of the different states of the residual stresses in the interfacial region, the initiation and propagation of the interfacial crack are different for the two composites. For example, the crack initiation and propagation behavior for an SCS-0 composite quenched from 500°C and having interfacial tensile and compressive fracture strengths of 700 and 3000 MPa, respectively, is as follows. As the transverse load is applied, the radial stresses at 0° become less compressive, while the hoop stresses at 90° become more tensile for both the matrix and interfacial region. When the transverse loading reaches 170 MPa, the hoop stresses in the interfacial region at 90° have exceeded the fracture strength (700 MPa) of the reaction product, leading to the formation of a radial crack at that location. Accompanied with the formation of this radial crack, the x-direction stresses in the interfacial region from 70° to 90° reduce dramatically simply because the hoop stress is released owing to the formation of the radial crack at 90°. In contrast, the x-direction stresses along the interface from 0° to 60° are increased, with the largest increment at 60° location. When the transverse loading is increased to 190 MPa, the x-direction stress at the interfacial region at 60° exceeds the fracture strength. Thus a tangential crack forms at that location and propagates immediately along the whole circumference of the interface. It is found that the detailed crack initiation and propagation for the SCS-0 composites also depend on the assumed interfacial fracture strength and the annealing temperature. For example, when the interfacial tensile fracture strength is set to be 800 MPa, the radial crack formed at 90° always triggers debonding of the whole interface immediately because the x-direction stress at the 60° location exceeds the fracture strength as soon as the radial crack forms at 90°.

The initiation and propagation of the interfacial crack for SCS-6 composites is quite different from that for SCS-0 composites. In this case, the crack is always initiated at the interfacial region located at about 30° to 45°. As soon as the crack is initiated, it propagates along the interface towards

0°, while the interfacial region from ~50° to 90° is still intact due to the presence of the residual compressive hoop and radial stresses. A higher stress than the crack initiation stress is needed to fail the whole interface. It should be pointed out that examination of the effective stresses for both types of composite studied indicates that no yielding of the matrix has occurred up to a transverse load of 450 MPa, even with total debonding of the interface. Because of this, the matrix plasticity has no effect on the initiation and propagation of the interfacial crack. Therefore, the different crack initiation and propagation behavior in the two composites is due to the different states of residual stress, which in turn is determined by the CTE mismatch between the fiber, the matrix and the interfacial region.

The present FEA indicates that debonding of the interface at different locations may not occur at the same stress level. As such, the external stresses that cause the interfacial debonding at the 30° location with respect to the transverse loading axis (referred to as the crack initiation stress hereafter) are summarized in Table 1. The interfacial region at 30° is selected because the integrity of this region dominates the back-reflected ultrasonic images. With this, a comparison between the ultrasonic experiment and the FEA can be made directly. It is noted from Table 1 that although the SCS-0 composites have a higher interfacial fracture strength (e.g. 800 MPa) than the SCS-6 composites (e.g. 300 MPa), the crack initiation stresses are almost the same for these two interfacial conditions. The reason for this lies in the different residual thermal stresses at the interfacial region. As discussed above, both the residual hoop and radial stresses at the interfacial region are in compression for the SCS-6 composites, whereas the residual hoop stress is in tension and the residual radial stress is in compression for the SCS-0 composites. Owing to the pre-existing tensile hoop stresses in the SCS-0 composite, a radial crack forms at 90° at a relatively low external stress. The formation of the radial crack leads to an early cracking at the 60° location that in turn triggers debonding of the whole interface. As such, the apparent crack initiation stress of the SCS-0 composites are similar to those of the SCS-6 composites,

although their interfacial fracture strengths are quite different. It is also noted that, as the quenching temperature decreases, the stress for crack initiation of the SCS-0 composites increases, and so does the stress for the decrease in the amplitude of the ultrasonic images. This result further supports the effect of the residual thermal stresses in the SCS-0 composites; i.e. the lower the quenching temperature, the lower the tensile hoop stress at the interfacial region, and therefore the higher the crack initiation stress.

Finally, it would be interesting to compare the present FEA results on single-fiber composites with those on high-volume-fiber composites. Our recent calculation for composites with a square array of 30 vol% SCS-0 and SCS-6 SiC fibers[23] indicates that the SCS-6 composites always debond first at the 30° to 45° locations, while the SCS-0 composites debond first at the 45° to 90° locations depending on the quenching temperature. The shifting of the crack initiation location from 90° to 45° in the SCS-0 composites corresponds to a decrease in the tensile hoop stress and compressive radial stress brought out by reducing the quenching temperature. Thus, the crack initiation and propagation behavior at the interface is very similar between composites with a single fiber and a high volume fraction of fibers, provided that they have the same interfacial properties. However, the stresses causing the debonding of the whole interface are quite different. Single-fiber composites require a higher stress to induce debonding of the whole interface than the corresponding high-volume-fiber composites. This is due to a larger residual radial stress present in the single-fiber composites than that in the high-volume-fiber composites.

Ultrasonic images of different interfaces

Ultrasonic images of a composite containing an SCS-0 fiber and an SCS-6 fiber under different loading are shown in *Figure 6* with the corresponding stress–strain curve. It can be seen that, for both the SCS-0 and SCS-6 interfaces, the amplitude of the back-reflected images remaines unaltered at the early stage of loading and then decreases at some locations of the interfaces as the far-field stress increases to about 300 MPa. Finally, the amplitude increases sharply as the stress reaches about 700 MPa. In addition to this non-monotonic stress dependence of the amplitude, several other phenomena can also be observed in *Figure 6*. (1) In the as-fabricated condition, the SCS-0 interface exhibits higher ultrasonic amplitudes than the SCS-6 interface; (2) under high stress loading (almost complete interfacial debond), the ultrasonic amplitudes of both the interfaces become almost the same; (3) the amplitude along the fiber axis varies with position; and (4) image separation exists at the two ends of the fiber.

The ultrasonic amplitude drops initially[15] corresponding to the occurrence of interfacial debonding, because the ultrasonic stresses reflected from the debonded and the bonded regions of the fiber destructively interfere with each other[14,15]. As the interfacial separation between the fiber and matrix increases after debonding, the amplitude begins to increases sharply because more and more debonded
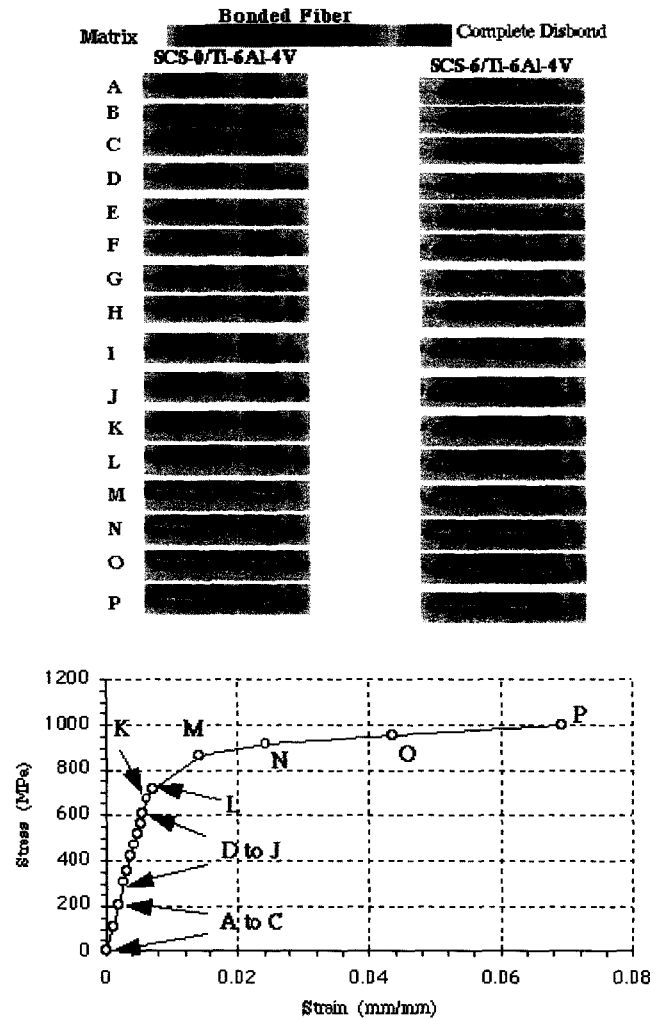

Figure 6 *In situ* ultrasonic imaging of the transverse test of a Ti–6Al–4V matrix composite made with SCS-0 and SCS-6 fibers. The SCS-0 fiber was broken during processing and shows as two separate pieces

region of the fiber is exposed to the ultrasonic stress wave with a corresponding reduction of bonded region seen by ultrasound. Finally, when most or all of the interface is debonded, the ultrasonic amplitudes from both SCS-0 and SCS-6 fibers will be similar.

A model developed previously[19,30] can be effectively used to describe the reason for similar amplitudes from fully debonded SCS-0 and SCS-6 interfaces even though, in as-made (untested) conditions, the SCS-0 interface always has a higher reflection amplitude than the SCS-6 interface at 25 MHz of ultrasonic frequency. The model[19,30] describes the ultrasonic shear back-reflection coefficient as a function of the interfacial elastic shear behavior at a given frequency of ultrasound, as shown in *Figure 7* (for 25 MHz of ultrasonic frequency). The result in *Figure 7* is obtained from the model which theoretically predicts the ultrasonic reflection coefficeint when shear waves are impingent on the fiber/matrix interface. The abscissa is the 'shear stiffness coefficient' which is zero for a complete debond and infinite for a completely rigid bond. In addition, the model allows for elastic (compliant) deformation of the interfacial region
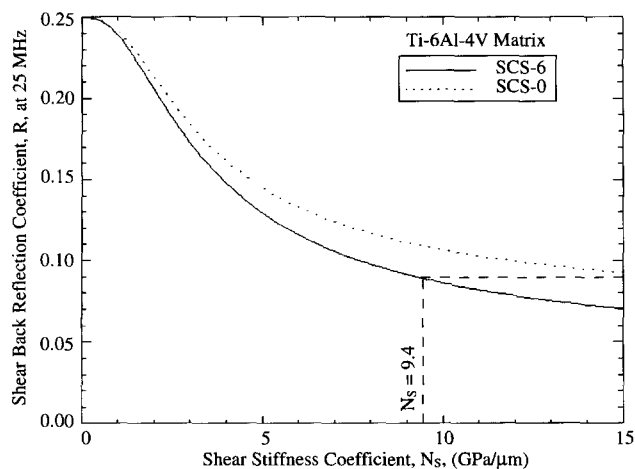
Figure 7 Ultrasonic shear reflection coefficient at 25 MHz as a function of shear stiffness coefficient for SCS-0 and SCS-6 interfaces in Ti–6Al–4V matrix

to represent the interphase zone formed by the chemical/metallurgical bond wherein the interfacial stiffness will fall between zero and infinity in an as-made sample. The ordinate in the figure is the ultrasonic reflection coefficient of the fiber/matrix interface represented on the abscissa. Subsequent to the theoretical modeling, experimental measurements have indicated[18] that, for a Ti–6Al–4V/SCS-6 interface, the shear stiffness coefficient is 9.4 GPa μm^{-1} and, therefore, the ultrasonic reflection coefficient from the SCS-0 will always be higher than that from SCS-6 except when there is a complete debond ($N_S = 0$). When the two interfaces (due to SCS-6 or SCS-0) debond, the ultrasonic amplitude is the highest and indentically same for the two interfaces. Further details of this aspect of modeling can be obtained from the literature[14,17–19,30].

Interfacial fracture strength

Since the commencement of the amplitude decrease is related to interfacial debonding, the interfacial fracture strength of the composites can be estimated by using the SBR data in conjunction with finite element analysis. The results from such a calculation are summarized in *Table 1*. As mentioned in the section on Finite Element Modeling, no time-dependent stress relaxation during cooling is considered in the FEA. Instead, some assumptions are made in this regard. For the SCS-6 composites quenched from 500 to 25°C, it is assumed that the composite is cooled instantly to 25°C. For the composite furnace-cooled from 930°C, it is assumed that 930°C furnace cooling is equivalent to 500°C water quenching, because the SCS-6 composites with these two cooling conditions exhibit similar stress levels for the onset of the decrease in the ultrasonic amplitude. For the composites furnace-cooled from 500°C, the equivalent quenching temperature is unknown. Thus, two different quenching temperatures (i.e. 300°C and 400°C) are evaluated to examine the effect of the residual thermal stresses. Another important aspect in the present FEA is the

cracking criterion for the fiber/matrix interfacial region, which is dependent on the tensile fracture strength and compressive strength of the coating or reaction products in the composites [see eqns (1) and (2)]. For most of the brittle materials, the ratio of the compressive strength to the tensile strength is typically in the range of 2 to 13[31]. Owing to the lack of strength data, the compressive strength of the interfacial region is set to be constant with 1000 MPa for the carbon coating and 3000 MPa for the uncoated interface.

Comparison between the FEA and SBR data suggests that the interfacial fracture strength of the SCS-0 composites is about 800 MPa because a fracture strength lower than 800 MPa (e.g. 600 or 700 MPa) would lead to crack initiation at a stress level of below 200 MPa (*Table 1*). The fracture strength of 800 MPa falls into the range of the observed modulus of rupture (507–855 MPa) for TiC bulk materials[32]. For the SCS-6 composites, an interfacial fracture strength of about 300 MPa is obtained from the current analysis. This fracture strength is higher than the estimation made by Nimmer *et al.*[28], who have concluded that the bond strength between SCS-6 fiber and Ti–6Al–4V matrix is near zero. However, our result is much closer to a recent report of the Ti–6Al–4V/SCS-6 SiC interfacial strength[33]. Using a newly designed, cross-shaped specimen geometry that can avoid the influence of singularity at the free surface of the interface and therefore is capable of providing the intrinsic interfacial fracture strength, Warrier *et al.*[33] have found that the fracture strength of the Ti–6Al–4V/SCS-6 SiC interface is about 115 MPa. Clearly, there still exists a discrepancy between the current study and the result from the cross-shaped specimens. It seems that the discrepancy is due to two reasons: one is the assumption of the elastic and thermal properties of the carbon coating in the FEA, and the other is the sensitivity of the ultrasonic imaging technique to the interfacial debonding. The change in response of the ultrasonic images to the debonding is gradual. Thus, the interfacial debonding may occur before the amplitude of the ultrasonic signal decrease becomes obvious. As such, the estimation made from the SBR data very likely represents the upper bound of the interfacial fracture strength.

CONCLUDING REMARKS

The present study has utilized finite element analysis in combination with an ultrasonic analysis technique, called the ultrasonic shear wave back-reflectivity technique, to assess the fracture strength of the fiber/matrix interfaces as well as to monitor the interfacial debonding and progression of the damage at the interfacial region in titanium-based MMCs under transverse loading conditions. Two interfacial conditions have been investigated. One is the Ti–6Al–4V/SCS-0 SiC interface, and the other is the Ti–6Al–4V/SCS-6 SiC interface. The finite element model used encompasses an interfacial element with a finite thickness and independent thermal and mechanical properties to simulate the interfacial region of the coating and/or reaction products. On the basis of data from the SBR and FEA, it is concluded

that the SCS-0 interface has a much higher fracture strength than the SCS-6 interface although both these interfaces display similar apparent debonding stresses.

REFERENCES

1. Charalambides, P.G. and Evans, A.G., Debonding properties of residually stressed brittle-matrix composites. *J. Am. Ceram. Soc.*, 1989, **72**, 746–753.
2. Kerans, R.J. and Parthasarathy, T.A., Theoretical analysis of the fiber pullout and pushout tests. *J. Am. Ceram. Soc.*, 1991, **74**, 1585–1596.
3. Marotzke, C., The elastic stress field arising in the single-fiber pull-out test. *Compos. Sci. Technol.*, 1994, **50**, 393–405.
4. Koss, D.A., Petrich, R.R., Kallas, M.N. and Hellmannn, J.R., Interfacial shear and matrix plasticity during fiber push-out in a metal-matrix composite. *Compos. Sci. Technol.*, 1994, **51**, 27–33.
5. Watson, M.C. and Clyne, T.W., The tensioned push-out test for fiber–matrix interface characterization under mixed mode loading. *Mater. Sci. Eng.*, 1993, **A160**, 1–5.
6. Hsueh, C.H., Analyses of slice compression tests for aligned ceramic matrix composites. *Acta Metall. Mater.*, 1993, **41**(12), 3585–3593.
7. Feillard, P., Desarmot, G. and Favre, J.P., Theoretical aspects of the fragmentation test. *Compos. Sci. Technol.*, 1994, **50**, 265–279.
8. Herrera-Franco, P.J., Rao, V., Drzal, L.T. and Chiang, M.Y.M., Bond strength measurement in composites—analysis of experimental techniques. *Compos. Eng.*, 1992, **2**(1), 31–45.
9. Karpur, P., Matikas, S., Krishnamurthy, S. and Ashbaugh, N. Ultrasound for fiber fragmentation size determination to characterize load transfer behavior of matrix–fiber interface in metal matrix composites. In '19th Annual Review of Progress in Quantitative Nondestructive Evaluation', Vol. 12B (Eds D.O. Thompson and D.E. Chimenti), Plenum, La Jolla, CA, 1992, pp. 1507–1513.
10. Waterbury, M.C., Karpur, P., Matikas, T.E., Krishnamurthy, S. and Miracle, D.B., *In situ* observation of the single fiber fragmentation process in metal matrix composites by ultrasonic imaging. *Compos. Sci. Technol.*, 1994, **52**(2), 261–266.
11. Folias, E.S., On the prediction of failure at a fiber/matrix interface in a composites subjected to a transverse tensile load. *J. Compos. Mater.*, 1991, **25**(7), 869–886.
12. Hu, S., Karpur, P., Matikas, T.E., Shaw, L. and Pagano, N.J., Free edge effect on residual stresses and debond of a composite fibre/matrix interface. *Mech. Compos. Mater. Struct.*, 1995, **2**, 215–225.
13. Pagano, N.J. in 'Local Mechanics Concepts for Composite Material Systems' (Eds J.N. Reddy and K.L. Reifsnider), Springer-Verlag, New York, 1991, pp. 1–26.
14. Karpur, P., Matikas, T.E., Shaw, L.L. and Miracle, D.B. A novel ultrasonic method of in-situ assessment of fracture and deformation of the fiber/matrix interface in metal-matrix composites. *Appl. Compos. Mater.* to be submitted.
15. Matikas, T.E., Karpur, P., Pagano, N. J., Hu, S. and Shaw, L. In-situ ultrasonic characterization of failure strength of fiber–matrix interface in metal matrix composites reinforced by SCS series fibers. In

16. Karpur, P. and Matikas, T.E. Theoretical modeling and experimental characterization of fiber–matrix interface in advanced composites. In '21th Annual Review of Progress in Quantitative Nondestructive Evaluation', Vol. 14B (Eds D.O. Thompson and D.E. Chimenti), Plenum, Snowmass Village, CO, 1994, pp. 1449–1456.
17. Matikas, T.E. and Karpur, P. Matrix–fiber interface characterization in metal matrix composites using ultrasonic shear-wave back-reflection coefficient technique. In '19th Review of Progress in Quantitative Nondestructive Evaluation', Vol. 12B (Eds D.O. Thompson and D.E. Chimenti), Plenum, La Jolla, CA, 1992, pp. 1515–1522.
18. Matikas, T.E. and Karpur, P. Micro-mechanics approach to characterize interfaces in metal and ceramic matrix composites. In '20th Annual Review of Progress in Quantitative Nondestructive Evaluation', Vol. 13B (Eds D.O. Thompson and D.E. Chimenti), Plenum, Bruswick, ME, 1993a, pp. 1477–1484.
19. Matikas, T.E. and Karpur, P., Ultrasonic reflectivity technique for the characterization of fiber–matrix interface in metal matrix composites. *J. Appl. Phys.*, 1993, **74**(1), 228–236.
20. Karpur, P., Matikas, T.E. and Krishnamurthy, S. Ultrasound as a tool for the development of aerospace structural titanium and ceramic matrix composites. In 'Proceedings of 1994 TMS Annual Meeting' (Eds R.Y. Lin and S.G. Fishman), The Minerals, Metals and Materials Society, San Francisco, CA, 1994, pp. 241–253.
21. Karpur, P., Stubbs, D.A., Matikas, T.E., Blodgett, M.P. and Krishnamurthy, S. Ultrasonic nondestructive characterization methods for the development and life prediction of titanium matrix composites. In 'Characterisation of Fiber Reinforced Titanium Matrix Composites', North Atlantic Treaty Organization, Bordeaux, France, 1993, pp. 13-1 to 13-12.
22. Metcalfe, A.G. in 'Interfaces in Metal Matrix Composites', Vol. 1 (Ed. A.G. Metcalf), Academic Press, New York, 1974, pp. 67–123.
23. Shaw, L. and Miracle D. Effects of an interfacial region on the transverse behavior of metal-matrix composites—a finite element analysis. *Acta Metall. Mater.* 1996, **44**(5), 2043–2055.
24. 'ANSYS User's Manual', Vols. I–IV, Swanson Analysis Systems, Inc., Houston, PA, 1992.
25. Adams, D.F. and Doner, D.R., Transverse normal loading of a unidirectional composite. *J. Compos. Mater.*, 1967, **1**(2), 152–164.
26. Dresselhaus, M.S., Dresselhaus, G., Sugihara, K., Spain, I.L. and Goldberg, H.A. 'Graphite Fibers and Filaments', Springer-Verlag, Berlin/Heidelberg, 1988.
27. Ziegler, G. and Huttner, W. in 'Engineered Materials Handbook: Ceramics and Glasses', Vol. 4 (Ed. S.J. Schneider), ASM International, 1991, pp. 835–844.
28. Nimmer, R.P., Bankert, R.J., Russell, E.S., Smith, G.A. and Wright, PK., Micromechanical modeling of fiber/matrix interface effects in transversely loaded SiC/Ti-6-4 metal matrix composites. *J. Compos. Technol. Res. (JCTRER)*, 1991, **13**(1), 3–13.
29. Nimmer, R.P., Fiber–matrix interface effects in the presence of thermally induced residual stresses. *J. Compos. Technol. Res. (JCTRER)*, 1990, **12**(2), 65–75.
30. Karpur, P., Matikas, T.E. and Krishnamurthy, S., Ultrasonic characterization of the fiber–matrix interphase/interface for mechanics of continuous fiber reinforced metal matrix and ceramic matrix composites. *J. Compos. Eng.*, 1995, **5**(6), 697–711.
31. Moore, R.E. in 'Engineered Materials Handbook: Ceramics and Glasses', Vol. 4 (Ed. S.J. Schneider), ASM International, 1991, pp. 747–891.
32. Benedict, T.L., Materials handbook for refractories, traditional, advanced ceramics. *Ceramic Industry*, 1994, **142**(1), 45–134.
33. Warrier, S.G., Gundel, D.B., Majumdar, B.S. and Miracle, D.B., Interface effects on the micromechanical response of a transversely loaded single fiber SCS-6/Ti–6Al–4V composite. *Metall. Mater. Trans.*, 1996, **27**(A), 2035–2043.